Multiple stiffening effects of nanoscale knobs on human red blood cells infected with *Plasmodium falciparum* malaria parasite

Yao Zhang[a], Changjin Huang[a], Sangtae Kim[b], Mahdi Golkaram[a], Matthew W. A. Dixon[c], Leann Tilley[c], Ju Li[b,d], Sulin Zhang[a,1], and Subra Suresh[e,f,g,1]

[a]Department of Engineering Science and Mechanics, The Pennsylvania State University, University Park, PA 16802; Departments of [b]Materials Science and Engineering and [d]Nuclear Science and Engineering, Massachusetts Institute of Technology, Cambridge, MA 02139; [c]Department of Biochemistry and Molecular Biology, Bio21 Molecular Science and Biotechnology Institute, The University of Melbourne, Melbourne, VIC 3010, Australia; and [e]Department of Materials Science and Engineering, [f]Department of Biomedical Engineering, and [g]Computational Biology Department, Carnegie Mellon University, Pittsburgh, PA 15213

During its asexual development within the red blood cell (RBC), *Plasmodium falciparum* (*Pf*), the most virulent human malaria parasite, exports proteins that modify the host RBC membrane. The attendant increase in cell stiffness and cytoadherence leads to sequestration of infected RBCs in microvasculature, which enables the parasite to evade the spleen, and leads to organ dysfunction in severe cases of malaria. Despite progress in understanding malaria pathogenesis, the molecular mechanisms responsible for the dramatic loss of deformability of *Pf*-infected RBCs have remained elusive. By recourse to a coarse-grained (CG) model that captures the molecular structures of *Pf*-infected RBC membrane, here we show that nanoscale surface protrusions, known as "knobs," introduce multiple stiffening mechanisms through composite strengthening, strain hardening, and knob density-dependent vertical coupling. On one hand, the knobs act as structural strengtheners for the spectrin network; on the other, the presence of knobs results in strain inhomogeneity in the spectrin network with elevated shear strain in the knob-free regions, which, given its strain-hardening property, effectively stiffens the network. From the trophozoite to the schizont stage that ensues within 24–48 h of parasite invasion into the RBC, the rise in the knob density results in the increased number of vertical constraints between the spectrin network and the lipid bilayer, which further stiffens the membrane. The shear moduli of *Pf*-infected RBCs predicted by the CG model at different stages of parasite maturation are in agreement with experimental results. In addition to providing a fundamental understanding of the stiffening mechanisms of *Pf*-infected RBCs, our simulation results suggest potential targets for antimalarial therapies.

red blood cells | malaria | coarse-grained simulations | shear modulus | stiffening

The most virulent human malaria parasite, *Plasmodium falciparum* (*Pf*), causes ~700,000 deaths each year (1, 2). Following entry into red blood cells (RBCs), the parasite matures through the ring (0–24 h), trophozoite (24–36 h), and schizont stages (40–48 h). This intraerythrocyte maturation is accompanied by striking changes in the surface topography and membrane architecture of the infected RBC (3–5). A notable modification is the formation of nanoscale protrusions, commonly known as knobs, at the RBC surface during the second half (24–48 h) of the asexual cycle. These protrusions mainly comprise the knob-associated histidine-rich protein (KAHRP) and the membrane-embedded cytoadherence protein, *Pf*-erythrocyte membrane protein 1 (PfEMP1). KAHRP binds to the fourth repeat unit of the spectrin α-chain, to ankyrin, to spectrin–actin–protein 4.1 complexes, and to the cytoplasmic domain of PfEMP (6–9). These attachments enhance the vertical coupling between the lipid bilayer and the spectrin network. Another striking modification in the *Pf*-infected RBC membrane is the

reorganization of the cytoskeletal network caused by parasite-induced actin remodeling (10). As a result of these molecular-level modifications, the *Pf*-infected RBC exhibits markedly increased stiffness [the shear modulus increases on average from ~4−10 μN/m in normal/uninfected RBCs, to ~40 μN/m at the trophozoite stage, and to as high as 90 μN/m at the schizont stage (11–13)] and cytoadherence to the vascular endothelium, which enable sequestration from circulation in vasculature, and evasion from the surveillance mechanisms of the spleen. Although in vitro experimental studies have revealed roles of particular parasite-encoded proteins in remodeling the host RBC (14–22), the mechanism by which *Pf*-infected RBCs gain dramatically increased stiffness has remained unclear. Indeed, uncertainty remains as to whether the loss of deformability arises from the structural reorganization of the host membrane components or from the deposition of parasite proteins. That is, it is not clear whether the stiffening is due to remodeling of the spectrin network, or to the formation of the knobs, or both. As experimental studies alone have heretofore not been able to determine the molecular details, numerical modeling, combined with a variety of experimental observations and measurements, offers an alternative approach to reveal the underlying mechanisms.

We present here a coarse-grained (CG) molecular dynamics (MD) RBC membrane model to correlate structural modifications at the molecular ultrastructure level with the shear responses of the *Pf*-infected RBC membrane, focusing on the second half of the parasite's intra-RBC asexual cycle (24–48 h), i.e., the

Significance

Our coarse-grained molecular dynamics (CGMD) simulations show that the deposition of nanoscale knobs, rather than spectrin network remodeling, is the primary cause of the dramatically increased stiffness of the *Plasmodium falciparum* (*Pf*)-infected red blood cell (RBC) membranes. Our analyses further reveal that the knobs stiffen the RBC membrane in a unique manner by simultaneously harnessing composite strengthening, strain hardening, and knob density-dependent vertical coupling effects. In addition to providing a fundamental understanding of the stiffening mechanism of *Pf*-infected RBCs, our simulation results suggest potential targets for antimalarial therapies.
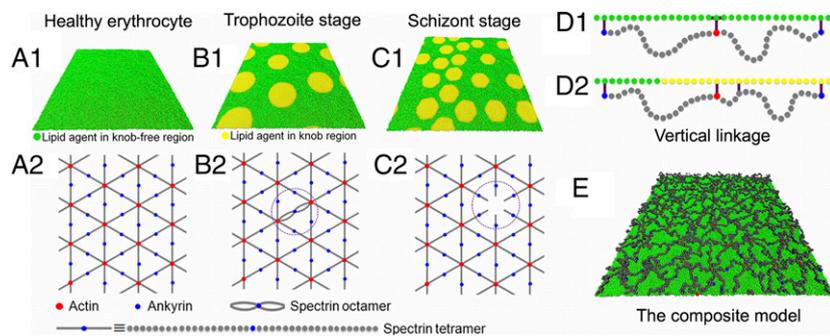
Fig. 1. A composite CG model of the human RBC membrane. (*A*–*C*) The one-agent–thick lipid bilayer model and the spectrin network model for uninfected (*A1* and *A2*), trophozoite-stage (*B1* and *B2*), and schizont-stage (*C1* and *C2*) RBCs, respectively. (*D*) Vertical associations between the overlying lipid bilayer and the spectrin network in normal (*D1*) and *Pf*-infected (*D2*) membranes. (*E*) The composite CG model integrating the lipid bilayer and the spectrin network. Green, normal lipid agents; yellow, lipid agents representing the knobby region; red, actin oligomers; blue, ankyrins; and gray, spectrin beads.

trophozoite and schizont stages. The CG model is computationally efficient, and able to capture the molecular structures of the RBC membrane in both normal and infected states. CGMD simulations reveal that spectrin network remodeling accounts for a relatively small change in shear modulus. Instead, the knobs stiffen the membrane by multiple mechanisms, including composite strengthening, strain hardening, and knob density-dependent vertical coupling. Our findings provide molecular-level understanding of the stiffening mechanisms operating in *Pf*-infected RBCs and shed light on the pathogenesis of falciparum malaria.

A Composite Model for Healthy and *Pf*-Infected RBC Membranes

The human RBC is one of the simplest cell types, comprising a lipid bilayer and an underlying spectrin network, coupled by integral membrane proteins. During its 120-d life span, the disk-shaped RBC (resting long diameter, ~8 μm) exhibits pronounced deformability and durability. It circulates approximately a million times in the human body, squeezing through narrow capillaries and the 1- to 2-μm interendothelial slits that separate the splenic cords and venous sinuses (23). Mechanically, the lipid bilayer of an uninfected RBC contributes to the out-of-plane bending resistance and helps maintain the membrane surface area, but cannot sustain in-plane static shear. The spectrin network is responsible for the shear modulus but possesses negligible bending rigidity. As such, many existing membrane models (24–33) reduce computational complexity by simulating only the lipid bilayer or the spectrin network, depending on the membrane deformation mode of interest. Such a simplification is well justified for the uninfected RBC membrane, but not for the *Pf*-infected RBC membrane, given its increased vertical coupling between the lipid bilayer and the spectrin network. Therefore, a composite RBC membrane model comprising both lipid bilayer and spectrin network with high computational efficiency is required.

Here, we formulate a composite CG RBC membrane model by integrating a one-agent–thick lipid bilayer model and a chain-of-bead spectrin network model via vertical connections that represent integral proteins (Fig. 1). Similar composite models have been developed, with variations in the lipid and spectrin representations (34–37). In the lipid bilayer model of a normal (uninfected) RBC membrane, a small patch of lipids in the lateral direction is coarse-grained into a single agent (Fig. 1*A1*). The agent carries not only translational but also orientational degrees of freedom. The interagent interaction is described by a simple pairwise potential that is dependent on both the interagent distance and orientation, which drives the self-assembly of the agents into a 2D fluid phase (38). This lipid bilayer model significantly improves the computational efficiency compared with the chain-of-bead lipid models, while faithfully capturing both the in-plane viscosity and out-of-plane bending rigidity of the lipid bilayer. In the spectrin network model (Fig. 1*A2*), spectrin tetramers and actin junctional complexes form a hexagonal spectrin network in the normal RBC membrane (39). Each spectrin

tetramer is modeled as a chain of 39 beads (40) [corresponding to the 39 triple-helical segments in a spectrin tetramer (41)], connected by unbreakable springs. Each vertex in the hexagonal network is an actin junctional complex at which an actin oligomer is linked to the beads at the end of six spectrin tetramers. The association between actin oligomers and spectrin tetramers is breakable and represented by a Lennard–Jones-type potential (40). To couple the lipid bilayer and the spectrin network, actin junctional complexes (representing protein 4.1–glycophorin C linkages) and the middle beads of spectrin tetramers (representing spectrin–ankyrin–band 3 linkages) are bonded to their closest lipid agents (Fig. 1*D1*). Further details of the models are provided in *SI Text*.

Two main modifications need to be taken into account in the model to simulate the *Pf*-infected RBC membrane: remodeling of the spectrin network due to the loss of actin oligomers, and the formation of the knobs and associated increase in vertical linkages to the lipid bilayer. Cryoelectron tomography experiments suggest substantive reorganization of the RBC cytoskeleton to generate actin filaments that tether organelles known as Maurer's clefts to the RBC membrane (10). Multiple filaments [each ~500 nm in length (10)] connect each of the Maurer's clefts [~15 in 3D7 parasites (42)] to the RBC cytoskeleton. Mining of the actin oligomers from the junctional complexes would result in reorganization of the spectrin network. To examine the likely consequences of actin mining, we examined the effect of having the same total number of spectrin tetramers converging on a reduced number of junction points, resulting in an enhanced spectrin network (Fig. 1*B2*). We also considered the effect of removing up to 20% of the junctional complexes, resulting in holes in the spectrin network (Fig. 1*C2*). Although other possibilities exist, these represent the extreme scenarios that give rise to the upper and lower bounds of the shear modulus, respectively. In the enhanced spectrin network, the network still maintains a perfect hexagonal arrangement. However, the distance between neighboring actin complexes (hence the end-to-end distance of the spectrin tetramers) is increased by 10% to keep the covered area unchanged from the normal network. Meanwhile, to keep the total number of spectrin heterodimers unchanged, 20% of spectrin tetramers are replaced by spectrin octamers. In the deficient spectrin network, some spectrin tetramers are disconnected in accordance with the loss of actin oligomers. According to a recent atomic force microscopy study of the RBC cytoskeleton (43), the enhanced spectrin network resembles the cytoskeleton of the *Pf*-infected RBCs at the trophozoite stage (Fig. 1*B2*), whereas the deficient spectrin network resembles that of the schizont stage (Fig. 1*C2*).

Another critical modification in the RBC membrane that needs to be incorporated into the model is the presence of the knobs. As the knob is enriched with proteins (KAHRP and PfEMP1), it can be regarded as a stiff nanosized domain with one end linked to the spectrin network and the other immersed in the lipid bilayer. The cross-sectional area and stiffness of the nanosized domain and its
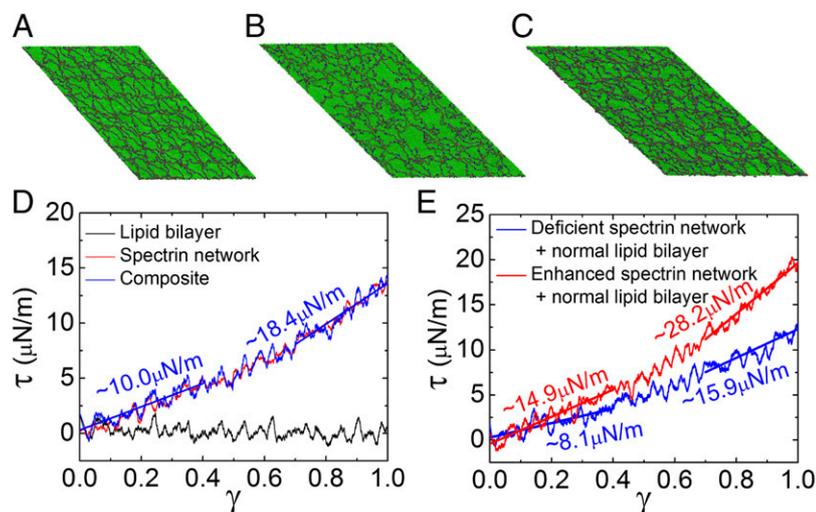
Fig. 2. Effects of spectrin network remodeling on the shear responses ($\dot{\gamma} = 2.97 \times 10^5 \mathrm{s}^{-1}$). (*A–C*) Sheared membranes at a shear strain $\gamma = 1$ for normal (*A*), deficient (*B*), and enhanced (*C*) spectrin networks, respectively. (*D*) Shear stress–strain responses of the uninfected RBC membrane, exhibiting strain-hardening behavior. (*E*) Shear responses of the RBC membrane with a normal lipid bilayer and a remodeled spectrin network.

connectivity to the spectrin network are key parameters governing its mechanical properties. In our simulations, instead of modeling the knobs as independent structures, we establish a biomechanically equivalent and computationally convenient model for the knobs. Specifically, each knob is modeled as a circular, relatively stiff lipid bilayer region (Fig. 1 *B1* and *C1*, yellow regions) that connects, whenever reachable, to the fourth beads of the nearest spectrin tetramers, to actin junctional complexes, and to ankyrins (Fig. 1*D2*), using harmonic springs. The potential well between a pair of lipid agents within the knob region is set to be deeper than that in the normal lipid bilayer so as to effectively stiffen it to capture the effective stiffness of the knob (see *SI Text* for details). Because the lipid bilayer region representing the knob has the same area and connectivity to the spectrin network and the replaced lipid domain contributes negligibly to the shear modulus, it is mechanically faithful to the real structure of the knob. In the course of parasite maturation, the density, size, and distribution of the knobs on the cell membrane dynamically change. Previous microstructural studies evidenced that in general the knob density increases, whereas the knob radius decreases from the trophozoite (Fig. 1*B1*) to the schizont (Fig. 1*C1*) stage (44, 45).

CG Simulations

To compute the shear modulus of the RBC membranes, a piece of RBC membrane ($\sim$600 nm $\times$ 600 nm) as shown in Fig. 1*E* was subjected to simple shear. Unless otherwise mentioned, the shear rate applied to the membrane was $\dot{\gamma} = 2.97 \times 10^5 \mathrm{s}^{-1}$, where γ is the engineering shear strain. As shall be seen later, such a shear rate is chosen so that the lipid bilayer in uninfected RBCs contributes negligibly to the shear stress (τ). Fig. 2*A* depicts the simulated configuration of the normal cell membrane at $\gamma = 1$. We found that only a small portion of the actin junctional complexes is broken. Fig. 2*D* shows the shear stress–strain responses of the uninfected RBC membrane. As expected, shearing generates negligible viscous stress in the lipid bilayer owing to its fluid nature, and the shear resistance is mainly contributed by the spectrin network. Notably, the spectrin network exhibits a strong strain-hardening effect, with a shear modulus of $\sim$10 μN/m at a small shear strain (<0.3) but of $\sim$18.4 μN/m at a high shear strain (>0.8). The extracted shear modulus of the healthy RBC thus falls within the range of existing experimental data [4$\sim$10 μN/m at small shear strain (<0.4); 14$\sim$20 μN/m at large shear strain ($\sim$1.0) (46, 47)].

The Effect of Spectrin Network Remodeling. We next investigate the role of spectrin network remodeling in the shear responses of *Pf*-infected RBC membranes. The simulation model comprises the normal lipid bilayer (Fig. 1*A1*) coupled with a spectrin network

that incorporates the proposed *Pf*-induced modifications (Fig. 1 *B2* or *C2*). For the deficient spectrin network (Figs. 1*C2* and 2*B*), the nonbonded tetramers do not sustain shear, and therefore, the shear modulus of the RBC membrane decreases to $\sim$8.1 and $\sim$15.9 μN/m at low and high shear strains, respectively (Fig. 2*E*). This reduction in the membrane shear modulus by the deficient spectrin network (i.e., with holes) might facilitate rupture of the RBC membrane during egress (48, 49). In contrast to the deficient spectrin network, the enhanced spectrin network maintains a perfect hexagonal topology upon shear (Fig. 2*C*). The shear modulus of the RBC membrane with the enhanced spectrin network is stiffened to $\sim$14.9 and $\sim$28.2 μN/m at low and high shear strains, respectively, as shown in Fig. 2*E*. The stiffness of each individual spectrin tetramer derived from the worm-like chain model (27) is positively correlated to its end-to-end distance. In addition, a spectrin octamer can be considered equivalent to two tetramers in parallel and consequently has a higher stiffness than a single tetramer. Thus, both the elongated end-to-end distance of spectrin tetramers and the emergence of the spectrin octamers contribute to the increase in shear modulus. However, the shear modulus (19.6 μN/m, averaged over the range of the shear strain from 0 to 1) caused by enhanced spectrin network is much less than that measured for *Pf*-infected RBC membranes [$\sim$40 μN/m at trophozoite stage and $\sim$60 μN/m at schizont stage on average (11, 13)]. Thus, mechanisms other than the spectrin network remodeling must be present for stiffening the *Pf*-infected RBC membrane.

The Effect of Knobs. The contribution of knobs to the stiffening of *Pf*-infected RBC membranes has been experimentally investigated by genetically eliminating KAHRP expression so as to prevent knob formation (50). It was shown that knobs account for $\sim$50% of the overall increase in the shear modulus in *Pf*-infected RBCs (50). However, it is possible that knocking out KAHRP also disrupts the transport of other parasite-encoded proteins. Additional proteins that might also contribute to the increased shear modulus include PfEMP3, RESA, MESA, Pf332, and STEVOR (17, 18, 20, 22, 51, 52). Our CG model is capable of separating the effect of the knobs from other factors. To this end, we establish a simulation model that combines the normal spectrin network with an overlying lipid bilayer that is modified with knobs. The knob density has been shown to vary between different human hosts (45), but the knob density increases as the intraerythrocytic parasite matures from the trophozoite to the schizont stage. Based on an ultrastructural study (44), we modeled the knob density to increase by 2.5 times as the intraerythrocytic parasite matures from the trophozoite to the schizont stage, from
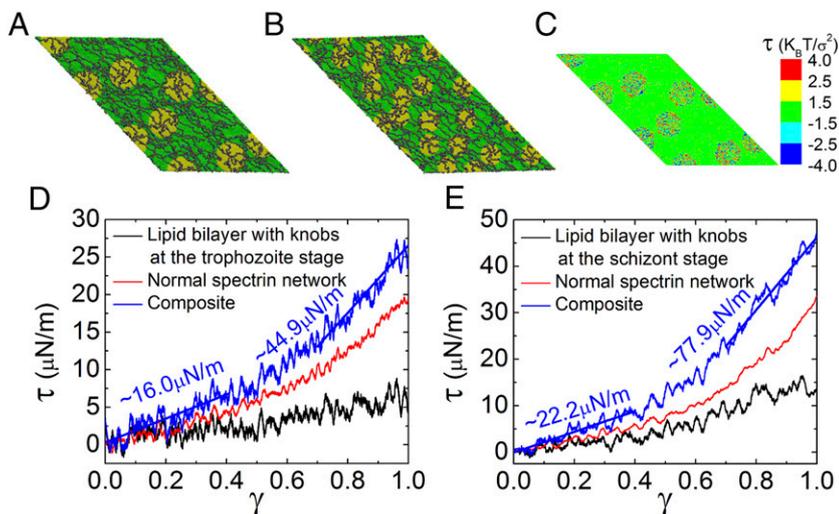
Fig. 3. The effects of knobs on the shear responses of the RBC membranes. (*A* and *B*) Simulation snapshots of sheared RBC membranes with knobs at the trophozoite and schizont stages for a shear strain $\gamma = 1$. Yellow regions represent knobs. (*C*) Shear stress profile in the lipid bilayer at $\gamma = 1$, showing that the knobby regions undergo appreciable shear stress. (*D* and *E*) Shear stress–strain responses of the RBC membrane with relevant knob sizes and densities at the trophozoite and schizont stages.

20 knobs per μm^2 (Fig. 1*B1*) to 50 knobs per μm^2 (Fig. 1*C1*). The average knob radius was modeled to decrease by 1.5 times, from 75 to 50 nm, and the ratio of the total knobby area to RBC membrane area slightly increased from 35% to 39% (44). From atomic force microscopy imaging (43), the center of each knob is roughly located on the top of an actin junctional complex but otherwise randomly positioned. Each knob forms vertical links by connecting to the actin junctional complex, and whenever reachable, to the fourth beads of the nearest spectrin tetramers, and to ankyrins. Following this connecting topology, each knob connects to the spectrin network by 8–11 vertical links for the knobs of size $r = 75$ nm and 6–8 vertical links for $r = 50$ nm; this gives rise to 73 total vertical links for the low-density large knobs and 147 for the high-density small ones. Note the twofold increase in the total number of vertical links due to the increase of the knob density, despite the small change of the total knob area.

Fig. 3 *A* and *B* display the shear morphologies of membranes with the knobs at trophozoite and schizont stages, respectively. Notably, as shown in Fig. 3*C*, the stiff lipid bilayer regions representing the knobs undergo finite shear stress, in contrast to the vanishing shear stress in the fluid lipid bilayer. Shear stresses in both the spectrin network and the knobby regions first rise slowly at low shear strains, and then sharply at large shear strains, corresponding to a pronounced stiffening effect. Our result indicates that the lipid domain representing the knobs no longer behaves as a Newtonian fluid, but more like a solid, which makes a considerable contribution to the shear modulus increase, as shown by the black curves in the figures. At $\gamma = 1$, the shear stress in the lipid bilayer makes up about 30% of the total shear stress, which is in clear contrast to the negligible viscous stress in the uninfected RBC membrane. The shear stress in the spectrin network also rises in the presence of knobs because of the enhanced vertical connections. At the trophozoite stage, the presence of knobs elevates the shear modulus of the RBC membrane to ~16.0 and ~44.9 $\mu N/m$ at low and high shear strains, respectively. Fig. 3*E* displays the shear stress–strain responses of the RBC membrane with knobs at the schizont stage, showing that the knob density significantly affects the shear modulus of the RBC membrane. The shear modulus is accordingly increased to ~22.2 and ~77.9 $\mu N/m$ at low and high shear strains, respectively.

Combined Effects. We next compute the shear moduli of *Pf*-infected RBC membranes at different asexual stages, combining the physiologically relevant spectrin network remodeling with different knob characteristics. Specifically, we combine the knob-stiffened mem-

brane bilayer with large knob size (Fig. 1*B1*) and the enhanced spectrin network (Fig. 1*B2*) to model the *Pf*-infected RBC membrane at the trophozoite stage. We also combine the lipid bilayer with small knob size (Fig. 1*C1*) and the deficient spectrin network (Fig. 1*C2*) to model the membrane at the schizont stage. Fig. 4 shows the shear stress–strain responses of the *Pf*-infected RBC membranes at the two later asexual stages, along with that of the uninfected membrane for comparison. At small shear strains, the shear modulus of the *Pf*-infected RBC membrane increases by twofold compared with the normal membrane. At large shear strains, the shear moduli of the *Pf*-infected RBC membrane at trophozoite and schizont stages are increased to ~48.1 and ~77.2 $\mu N/m$, respectively. Compared with the cases with physiologically relevant knob radii and densities but with normal spectrin network (Fig. 3 *D* and *E*), the shear moduli of the *Pf*-infected RBC membranes change negligibly, further demonstrating the insignificant role of the spectrin network remodeling on stiffening. The shear moduli predicted by this model at both small and large shear strains for these two stages fall in the range of experimental measurements [20~60 $\mu N/m$ at trophozoite stage; 25~90 $\mu N/m$ at schizont stage (11, 13)].
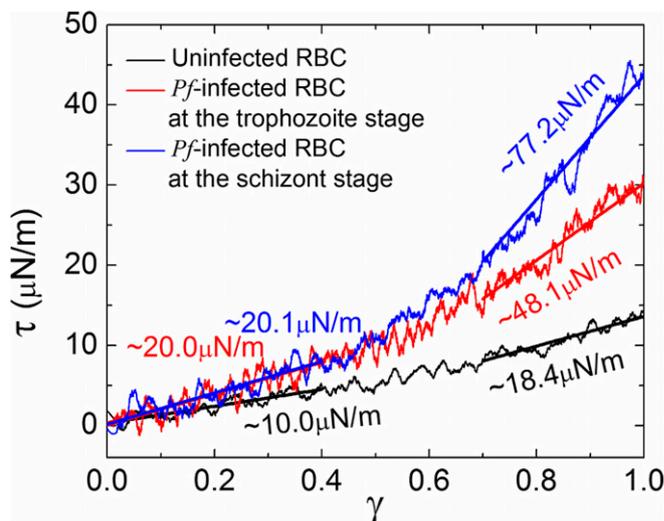

Fig. 4. Shear stress–strain responses of uninfected (black line) and *Pf*-infected RBC membranes at the trophozoite (red line) and schizont (blue line) stages.
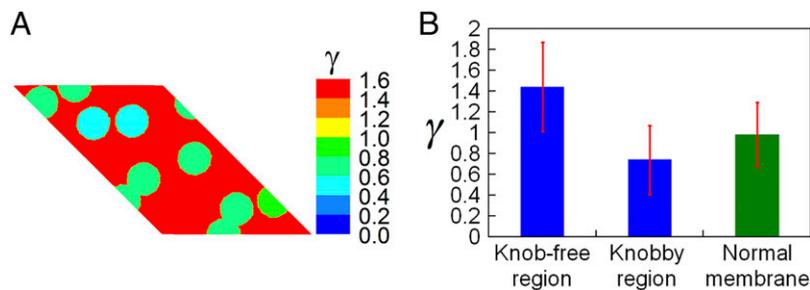
Fig. 5. Stiffening due to the inhomogeneous strain induced by the presence of the knobs ($\alpha = 0.35$). (*A*) Inhomogeneous shear strain distribution in the spectrin network. The shear strain in the knob-free regions is much higher than that applied, representing a stiffening mechanism due to the strain-hardening property of the spectrin network. (*B*) The average shear strain in the knob-free regions is $\gamma_F = 1.44$, whereas that in the knobby regions is $\gamma_K = 0.74$ at an applied shear strain $\gamma_C = 1$. The shear strain in the normal spectrin network (without knobs) is homogeneous and consistent with the applied shear strain.

Analysis

We view the knobby RBC membrane as a composite with two regions: one with the spectrin network only (knob-free region) and the other with the spectrin network with attached knobs. Because the fluid lipid bilayer does not contribute to shear resistance, it is not considered in the analysis. According to the rule of mixtures, the shear strain applied to the composite γ_C is distributed in the two domains,

$$\gamma_C = \alpha \gamma_K + (1 - \alpha)\gamma_F, \quad [1]$$

where γ_F and γ_K are the shear strains in the knob-free spectrin network region and the knobby region, respectively, and α is the areal fraction of the knobby region. Because these two regions are subjected to the same shear stress τ,

$$\tau = \gamma_K G_K = \gamma_F G_F(\gamma_F), \quad [2]$$

where G_F and G_K are the shear moduli of the knob-free and the knobby regions, respectively. To emphasize the material nonlinearity and strain-hardening effects of the spectrin network, the shear modulus of the spectrin network is expressed here as a function of the shear strain γ_F. Substituting Eq. **2** to Eq. **1** and noting that the protein-enriched knobby region is much more rigid than the spectrin network ($G_K \gg G_F$), one arrives at the conclusion that the shear strain in the knob-free region is amplified by a factor of approximately $1/(1 - \alpha)$ from the applied shear strain:

$$\gamma_F = \frac{\gamma_C}{[\alpha G_F(\gamma_F)/G_K + (1 - \alpha)]} \approx \gamma_C/(1 - \alpha). \quad [3]$$

This suggests that the knob-free region experiences an elevated strain (γ_F) compared with the apparent, applied shear strain (γ_C). This amplified shear strain in the knob-free region is confirmed by our CG simulations, as shown in Fig. 5, where $\gamma_F = 1.44$ for $\gamma_C = 1$ and $\alpha = 0.35$. Rule of mixtures gives rise to the shear modulus of the composite as follows:

$$\frac{1}{G_C(\gamma_C)} = \frac{\alpha}{G_K} + \frac{1 - \alpha}{G_F(\gamma_C/(1 - \alpha))}. \quad [4]$$

The expression of the shear modulus of the *Pf*-infected RBC membranes thus manifests as a dual stiffening mechanism of the knob-membrane complexes. First, the knobs act as structural strengtheners of the spectrin network, as represented by the first term on the right side of Eq. 4. Second, the presence of rigid knobs results in inhomogeneous shear strain distribution. In particular, the shear strain in the knob-free regions is amplified compared with the externally applied shear strain ($\gamma_F > \gamma_C$). Owing to the strain-hardening property of the spectrin network, $G_F(\gamma_F) > G_F(\gamma_C)$, the knob-free regions are also effectively stiffened, as indicated in the second term of Eq. 4. For an applied shear strain $\gamma = 1$, the expected shear modulus of the knob-free region is ∼50 μN/m, compared with ∼20 μN/m without the strain-hardening effect (see Fig. S1 for shear modulus at high shear strains). The dual role of the knobs explains the significantly increased shear modulus of *Pf*-infected RBC membranes.

Our simulations further revealed that the strong knob density (or size) effect originates from the increase in the total number of vertical links from the knobs to the spectrin network through a comparative study, as detailed in *SI Text*. In the case of the same total knobby area and the same total number of vertical links but different knob size [thus different knob density (Fig. S2)], the shear modulus changes negligibly. Whereas for the same knob size but with the increase in the total knobby area and hence in the total number of vertical links, the shear stiffness markedly increases (Fig. S3). These comparative studies demonstrate that the total number of vertical links, rather than the apparent knob size or the total knobby area, is a primary stiffening factor. From the trophozoite to the schizont stage, the total knobby area remains roughly the same, but the knob density increases. As a result, the total number of vertical links increases and a much stiffer membrane develops. It is interesting to consider how the parasite could stiffen the membrane by remodeling the knob size and density so as to increase the vertical coupling to the spectrin network to stiffen the membrane.

Discussion and Concluding Remarks

We have developed an efficient composite RBC membrane model of the lipid bilayer and the spectrin cytoskeleton network. This model enables a systematic study of the effects of changes in the molecular structures on the shear elasticity of *Pf*-infected RBC membranes. Our modeling results show that the deposition of knobs, rather than spectrin network remodeling, is the primary cause of the dramatically increased stiffness of the *Pf*-infected RBC membranes. Our analysis further revealed that the knobs stiffen the RBC membrane in a unique manner by simultaneously harnessing composite strengthening, strain hardening, and knob density-dependent vertical coupling effects. First, the knobs stiffen the spectrin network as structural strengtheners, commonly seen in composites reinforced by stiff inclusions. Second, the presence of knobs significantly elevates the shear strain in the knob-free regions of the spectrin network; given the strain-hardening property of the spectrin network, the knob-free regions are also effectively stiffened. Third, during maturation from the trophozoite to the schizont stage, the knob density increases, resulting in increased number of the knob-associated vertical links, which further increases the membrane stiffness. The predicted shear moduli of *Pf*-infected RBC membranes by the CG model fall in the range of the experimental measurements [20∼60 μN/m at trophozoite stage; 25∼90 μN/m at schizont stage (11, 13)].

The present study suggests possible targets for the development of effective antimalarial agents. The cytoadherence protein, PfEMP1 (53, 54), has been previously suggested (55) as

promising target molecules for developing medication against malaria. Disrupting the PfEMP1 proteins would undoubtedly reduce the cytoadherence, but it might not be effective for changing the high stiffness of the membrane. In addition to the stiffening role, the knobs also act as platforms for the presentation of PfEMP1. The high stiffness of the knobby region together with the knob-associated vertical connections facilitate the distribution of the tensional forces imposed on PfEMP1 to the entire knobby region and to the cytoskeleton. In light of these multifunctional roles, disrupting the vertical proteins would potentially reduce both the stiffness and the strength of adhesion to the endothelium. Molecules that block the binding of KAHRP (or other parasite-encoded proteins) to RBC spectrin network could be promising candidates as antimalarial agents.

1. Murray CJL, et al. (2012) Global malaria mortality between 1980 and 2010: A systematic analysis. *Lancet* 379(9814):413–431.
2. Hay SI, et al. (2009) A world malaria map: *Plasmodium falciparum* endemicity in 2007. *PLoS Med* 6(3):e1000048.
3. Maier AG, Cooke BM, Cowman AF, Tilley L (2009) Malaria parasite proteins that remodel the host erythrocyte. *Nat Rev Microbiol* 7(5):341–354.
4. Bannister LH, Hopkins JM, Fowler RE, Krishna S, Mitchell GH (2000) A brief illustrated guide to the ultrastructure of *Plasmodium falciparum* asexual blood stages. *Parasitol Today* 16(10):427–433.
5. Haldar K, Mohandas N (2007) Erythrocyte remodeling by malaria parasites. *Curr Opin Hematol* 14(3):203–209.
6. Pei X, et al. (2005) Structural and functional studies of interaction between *Plasmodium falciparum* knob-associated histidine-rich protein (KAHRP) and erythrocyte spectrin. *J Biol Chem* 280(35):31166–31171.
7. Magowan C, et al. (2000) *Plasmodium falciparum* histidine-rich protein 1 associates with the band 3 binding domain of ankyrin in the infected red cell membrane. *Biochim Biophys Acta* 1502(3):461–470.
8. Waller KL, Cooke BM, Nunomura W, Mohandas N, Coppel RL (1999) Mapping the binding domains involved in the interaction between the *Plasmodium falciparum* knob-associated histidine-rich protein (KAHRP) and the cytoadherence ligand *P. falciparum* erythrocyte membrane protein 1 (PfEMP1). *J Biol Chem* 274(34):23808–23813.
9. Oh SS, et al. (2000) Plasmodium falciparum erythrocyte membrane protein 1 is anchored to the actin-spectrin junction and knob-associated histidine-rich protein in the erythrocyte skeleton. *Mol Biochem Parasitol* 108(2):237–247.
10. Cyrklaff M, et al. (2011) Hemoglobins S and C interfere with actin remodeling in *Plasmodium falciparum*-infected erythrocytes. *Science* 334(6060):1283–1286.
11. Suresh S (2006) Mechanical response of human red blood cells in health and disease: Some structure-property-function relationships. *J Mater Res* 21(08):1871–1877.
12. Suresh S, et al. (2005) Connections between single-cell biomechanics and human disease states: Gastrointestinal cancer and malaria. *Acta Biomater* 1(1):15–30.
13. Park Y, et al. (2008) Refractive index maps and membrane dynamics of human red blood cells parasitized by *Plasmodium falciparum*. *Proc Natl Acad Sci USA* 105(37):13730–13735.
14. Maier AG, et al. (2008) Exported proteins required for virulence and rigidity of *Plasmodium falciparum*-infected human erythrocytes. *Cell* 134(1):48–61.
15. Rug M, Prescott SW, Fernandez KM, Cooke BM, Cowman AF (2006) The role of KAHRP domains in knob formation and cytoadherence of *P. falciparum*-infected human erythrocytes. *Blood* 108(1):370–378.
16. Mills JP, et al. (2007) Effect of plasmodial RESA protein on deformability of human red blood cells harboring *Plasmodium falciparum*. *Proc Natl Acad Sci USA* 104(22):9213–9217.
17. Diez-Silva M, et al. (2012) Pf155/RESA protein influences the dynamic microcirculatory behavior of ring-stage *Plasmodium falciparum* infected red blood cells. *Sci Rep* 2:614.
18. Pei X, Guo X, Coppel R, Mohandas N, An X (2007) *Plasmodium falciparum* erythrocyte membrane protein 3 (PfEMP3) destabilizes erythrocyte membrane skeleton. *J Biol Chem* 282(37):26754–26758.
19. Pei X, et al. (2007) The ring-infected erythrocyte surface antigen (RESA) of *Plasmodium falciparum* stabilizes spectrin tetramers and suppresses further invasion. *Blood* 110(3):1036–1042.
20. Hodder AN, et al. (2009) Analysis of structure and function of the giant protein Pf332 in *Plasmodium falciparum*. *Mol Microbiol* 71(1):48–65.
21. Orjih AU, Cherian PT (2013) Possible relationship between *Plasmodium falciparum* ring-infected erythrocyte surface antigen (RESA) and host cell resistance to destruction by chemicals. *Parasitol Res* 112(12):4043–4051.
22. Glenister FK, et al. (2009) Functional alteration of red blood cells by a megadalton protein of *Plasmodium falciparum*. *Blood* 113(4):919–928.
23. An X, Mohandas N (2008) Disorders of red cell membrane. *Br J Haematol* 141(3):367–375.
24. Boal DH (1994) Computer simulation of a model network for the erythrocyte cytoskeleton. *Biophys J* 67(2):521–529.
25. Boey SK, Boal DH, Discher DE (1998) Simulations of the erythrocyte cytoskeleton at large deformation. I. Microscopic models. *Biophys J* 75(3):1573–1583.
26. Discher DE, Boal DH, Boey SK (1998) Simulations of the erythrocyte cytoskeleton at large deformation. II. Micropipette aspiration. *Biophys J* 75(3):1584–1597.
27. Li J, Dao M, Lim CT, Suresh S (2005) Spectrin-level modeling of the cytoskeleton and optical tweezers stretching of the erythrocyte. *Biophys J* 88(5):3707–3719.
28. Gov NS (2007) Active elastic network: Cytoskeleton of the red blood cell. *Phys Rev E Stat Nonlin Soft Matter Phys* 75(1 Pt 1):011921.
29. Noguchi H, Gompper G (2005) Shape transitions of fluid vesicles and red blood cells in capillary flows. *Proc Natl Acad Sci USA* 102(40):14159–14164.
30. McWhirter JL, Noguchi H, Gompper G (2009) Flow-induced clustering and alignment of vesicles and red blood cells in microcapillaries. *Proc Natl Acad Sci USA* 106(15):6039–6043.
31. Pivkin IV, Karniadakis GE (2008) Accurate coarse-grained modeling of red blood cells. *Phys Rev Lett* 101(11):118105.
32. Fedosov DA, Caswell B, Suresh S, Karniadakis GE (2011) Quantifying the biophysical characteristics of *Plasmodium-falciparum*-parasitized red blood cells in microcirculation. *Proc Natl Acad Sci USA* 108(1):35–39.
33. Fedosov DA, Caswell B, Karniadakis GE (2010) A multiscale red blood cell model with accurate mechanics, rheology, and dynamics. *Biophys J* 98(10):2215–2225.
34. Li H, Lykotrafitis G (2014) Erythrocyte membrane model with explicit description of the lipid bilayer and the spectrin network. *Biophys J* 107(3):642–653.
35. Peng Z, et al. (2013) Lipid bilayer and cytoskeletal interactions in a red blood cell. *Proc Natl Acad Sci USA* 110(33):13356–13361.
36. Sikder MKU, Stone KA, Kumar PBS, Laradji M (2014) Combined effect of cortical cytoskeleton and transmembrane proteins on domain formation in biomembranes. *J Chem Phys* 141(5):054902.
37. Spangler EJ, Harvey CW, Revalee JD, Kumar PBS, Laradji M (2011) Computer simulation of cytoskeleton-induced blebbing in lipid membranes. *Phys Rev E Stat Nonlin Soft Matter Phys* 84(5 Pt 1):051906.
38. Yuan H, Huang C, Li J, Lykotrafitis G, Zhang S (2010) One-particle-thick, solvent-free, coarse-grained model for biological and biomimetic fluid membranes. *Phys Rev E Stat Nonlin Soft Matter Phys* 82(1 Pt 1):011905.
39. Liu SC, Derick LH, Palek J (1987) Visualization of the hexagonal lattice in the erythrocyte membrane skeleton. *J Cell Biol* 104(3):527–536.
40. Li J, Lykotrafitis G, Dao M, Suresh S (2007) Cytoskeletal dynamics of human erythrocyte. *Proc Natl Acad Sci USA* 104(12):4937–4942.
41. Bennett V, Baines AJ (2001) Spectrin and ankyrin-based pathways: Metazoan inventions for integrating cells into tissues. *Physiol Rev* 81(3):1353–1392.
42. Dixon MWA, et al. (2011) Genetic ablation of a Maurer's cleft protein prevents assembly of the *Plasmodium falciparum* virulence complex. *Mol Microbiol* 81(4):982–993.
43. Shi H, et al. (2013) Life cycle-dependent cytoskeletal modifications in *Plasmodium falciparum* infected erythrocytes. *PLoS One* 8(4):e61170.
44. Gruenberg J, Allred DR, Sherman IW (1983) Scanning electron microscope-analysis of the protrusions (knobs) present on the surface of *Plasmodium falciparum*-infected erythrocytes. *J Cell Biol* 97(3):795–802.
45. Quadt KA, et al. (2012) The density of knobs on *Plasmodium falciparum*-infected erythrocytes depends on developmental age and varies among isolates. *PLoS One* 7(9):e45658.
46. Mills JP, Qie L, Dao M, Lim CT, Suresh S (2004) Nonlinear elastic and viscoelastic deformation of the human red blood cell with optical tweezers. *Mech Chem Biosyst* 1(3):169–180.
47. Dao M, Li J, Suresh S (2006) Molecularly based analysis of deformation of spectrin network and human erythrocyte. *Mater Sci Eng C* 26(8):1232–1244.
48. Chandramohanadas R, et al. (2009) Apicomplexan parasites co-opt host calpains to facilitate their escape from infected cells. *Science* 324(5928):794–797.
49. Chandramohanadas R, et al. (2011) Biophysics of malarial parasite exit from infected erythrocytes. *PLoS One* 6(6):e20869.
50. Glenister FK, Coppel RL, Cowman AF, Mohandas N, Cooke BM (2002) Contribution of parasite proteins to altered mechanical properties of malaria-infected red blood cells. *Blood* 99(3):1060–1063.
51. Waller KL, et al. (2003) Mature parasite-infected erythrocyte surface antigen (MESA) of *Plasmodium falciparum* binds to the 30-kDa domain of protein 4.1 in malaria-infected red blood cells. *Blood* 102(5):1911–1914.
52. Sanyal S, et al. (2012) Plasmodium falciparum STEVOR proteins impact erythrocyte mechanical properties. *Blood* 119(2):e1–e8.
53. Ho M, White NJ (1999) Molecular mechanisms of cytoadherence in malaria. *Am J Physiol* 276(6 Pt 1):C1231–C1242.
54. Carvalho PA, Diez-Silva M, Chen H, Dao M, Suresh S (2013) Cytoadherence of erythrocytes invaded by *Plasmodium falciparum*: Quantitative contact-probing of a human malaria receptor. *Acta Biomater* 9(5):6349–6359.
55. Beeson JG, Chan JA, Fowkes FJI (2013) PfEMP1 as a target of human immunity and a vaccine candidate against malaria. *Expert Rev Vaccines* 12(2):105–108.

BIOPHYSICS AND COMPUTATIONAL BIOLOGY